

45.5-tesla direct-current magnetic field generated with a high-temperature superconducting magnet

Seungyong Hahn^{1,2}, Kwanglok Kim¹, Kwangmin Kim¹, Xinbo Hu¹, Thomas Painter¹, Iain Dixon¹, Seokho Kim^{1,3}, Kabindra R. Bhattarai^{1,4}, So Noguchi^{1,5}, Jan Jaroszynski¹ & David C. Larbalestier^{1,4*}

Strong magnetic fields are required in many fields, such as medicine (magnetic resonance imaging), pharmacy (nuclear magnetic resonance), particle accelerators (such as the Large Hadron Collider) and fusion devices (for example, the International Thermonuclear Experimental Reactor, ITER), as well as for other diverse scientific and industrial uses. For almost two decades, 45 tesla has been the highest achievable direct-current (d.c.) magnetic field; however, such a field requires the use of a 31-megawatt, 33.6-tesla resistive magnet inside 11.4-tesla low-temperature superconductor coils¹, and such high-power resistive magnets are available in only a few facilities worldwide². By contrast, superconducting magnets are widespread owing to their low power requirements. Here we report a high-temperature superconductor coil that generates a magnetic field of 14.4 tesla inside a 31.1-tesla resistive background magnet to obtain a d.c. magnetic field of 45.5 tesla—the highest field achieved so far, to our knowledge. The magnet uses a conductor tape coated with REBCO ($\text{REBa}_2\text{Cu}_3\text{O}_x$, where RE = Y, Gd) on a 30-micrometre-thick substrate³, making the coil highly compact and capable of operating at the very high winding current density of 1,260 amperes per square millimetre. Operation at such a current density is possible only because the magnet is wound without insulation⁴, which allows rapid and safe quenching from the superconducting to the normal state^{5–10}. The 45.5-tesla test magnet validates predictions¹¹ for high-field copper oxide superconductor magnets by achieving a field twice as high as those generated by low-temperature superconducting magnets.

Besides its no-insulation construction, the magnet design is mostly conventional, as described in Methods. Table 1 summarizes the key

design parameters of our REBCO tape and magnet. The magnet (Fig. 1), named ‘little big coil’ (LBC), consists of a stack of 12 single pancake coils (hereafter ‘pancakes’) wound with 4.02-mm-wide and 43- μm -thick REBCO tape. The tape is composed of a thin 30- μm -thick Hastelloy C-276 substrate, 1.5 μm of REBCO, a thin silver coating and a final hermetic 5- μm -thick electroplated copper stabilizer, manufactured by SuperPower, Inc. Such thin substrate tapes only became available recently but they immediately attracted our attention because they could enable a very compact and mechanically strong winding. The effective Young’s moduli E shown in Table 1 benefit greatly from the high ratio of Hastelloy ($E = 210$ GPa) to Cu ($E = 100$ GPa) content of the winding.

The coil was the third in a series of LBCs, with LBC1 reaching 40 T, LBC2 attaining 42.5 T and LBC3 achieving 45.5 T, all in the same 31.1-T background field and all with nominally the same design. We found that tests in liquid nitrogen were valuable for checking joint resistances and establishing key operation parameters, including the coil constant, the characteristic coil resistance, R_c , and the charging time constant^{12–15}. Occasionally some joints were remade to reduce resistive losses and minimize coil warming during test. For the high-field test, LBC3 was placed in a 37-mm-diameter liquid helium cryostat inside the resistive background magnet (50-mm warm bore, 18 MW, 31.1 T) at the National High Magnetic Field Laboratory (MagLab). To mitigate trapped helium bubbles, which allow heating of the magnet above 4.2 K during charging¹⁶, a small-diameter tube above the magnet periodically pumped away helium vapour during the test so as to limit the temperature of the top surface of LBC3, which reached 7 K at the moment of the 45.5-T quench. A Hall sensor calibrated up to 44.8 T in the 45-T

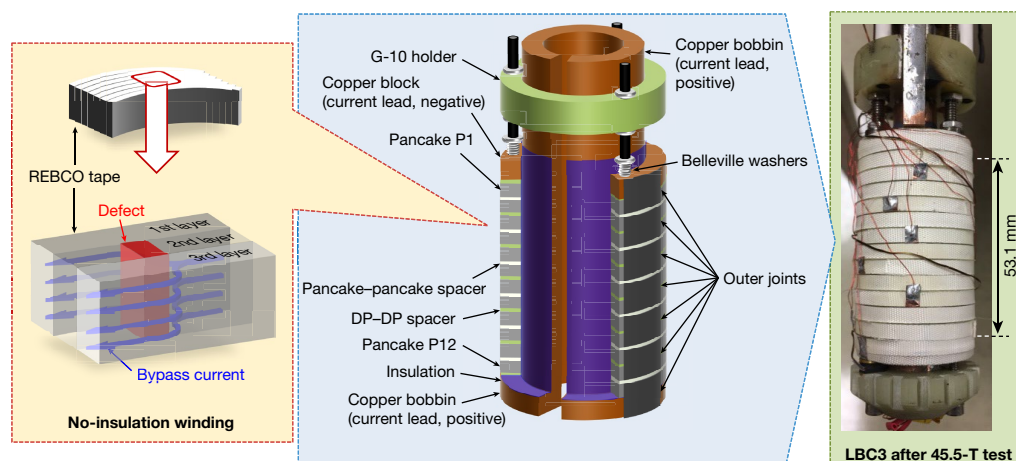


Fig. 1 | Design and construction of LBC. Left, principle of the no-insulation technique. Centre, construction design of LBC (not to scale). Right, Photograph of LBC. Owing to the no-insulation technique, any dissipative region is bypassed by current transfer to adjacent turns.

Because of this vital ‘current-sharing’ feature, electrical burn-out—often observed in ‘insulated’ high-field HTS coils—was not observed after the 45.5-T quench, even at the extremely high conductor current density of 1,420 A mm⁻².

¹National High Magnetic Field Laboratory, Florida State University, Tallahassee, FL, USA. ²Department of Electrical and Computer Engineering, Seoul National University, Seoul, South Korea.

³Department of Mechanical Engineering, Changwon National University, Changwon, South Korea. ⁴Department of Mechanical Engineering, FAMU-FSU College of Engineering, Tallahassee, FL, USA.

⁵Graduate School of Information Science and Technology, Hokkaido University, Sapporo, Japan. *e-mail: larbalestier@asc.magnet.fsu.edu

Table 1 | Key parameters of LBC, its conductor and the outer 31-T resistive magnet

Parameters	Values
REBCO tape	
Width; thickness	4.02 mm; 0.043 mm
Thickness of substrate; thickness of copper	0.03 mm; 0.01 mm
Effective Young's moduli, E_r ; E_h ; E_z	69 GPa; 144 GPa; 144 GPa
LBC	
Winding inner diameter; outer diameter; height	14 mm; 34 mm; 53.1 mm
Number of pancakes	12
Turns per single pancake	226.4 (average)
Total number of turns	2,717
Magnet constant	59.7 mT A ⁻¹
Total inductance	50.4 mH
Characteristic resistance, R_c	47.1 mΩ
Charging time constant	1.07 s
31-T background magnet	
Magnet constant	0.843 mT A ⁻¹
Self-inductance	4.30 mH
Mutual inductance with LBC	1.09 mH

hybrid magnet was used to measure the centre field, together with a pickup coil (the linearity of which was confirmed in multiple charging tests before the main 45.5-T test). Figure 2 shows the measured central field of 45.5 T at an LBC3 quench current of 245.3 A and a conductor current density of 1,420 A mm⁻². This field is 0.2 T lower than the field of 45.7 T, which was calculated using the designed magnet constant of 59.7 mT A⁻¹ and the measured background field of 31.1 T. A centre field discrepancy between measurement and calculation is typically observed in high-temperature superconductor (HTS) magnets owing to diamagnetic screening currents that lower the transport-current field^{17–23}. We also took into account a turn-to-turn leakage current of 0.2 A, calculated from the measured overall coil voltage of 9.45 mV and the measured characteristic resistance of 47.1 mΩ, which corresponds²⁴ to a centre field of 12 mT. LBC3 was ‘dry-wound’—that is, the coil was free of epoxy or any other encapsulant and the individual turns within the winding were essentially ‘self-supporting’, with a hoop stress of $\sigma_0 = BJR$, where B is the field, J is the conductor current density and R is the local radius. The peak magnetic stress was estimated to be 691 MPa, and the sum of the magnetic and bending strains was 0.38%.

The 45.5-T quench field of LBC3 is the highest d.c. field reported until now, slightly exceeding the 45-T field of the hybrid magnet at MagLab¹, which has been serving MagLab users since 2000, and higher than the 40-T field of LBC1 and 42.5-T field of LBC2 thanks to small

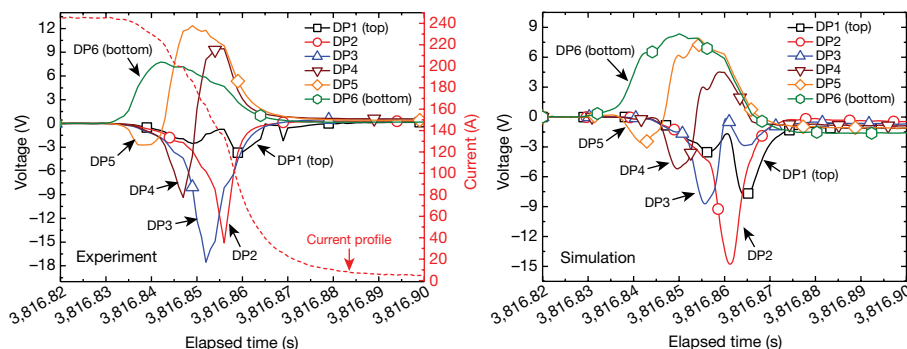


Fig. 3 | Voltages of DPs during the quench of LBC3 at 45.5 T. Left, Measured voltages. Right, Simulated voltages. The simulation used a previously validated lumped circuit model²⁶. The quench was initiated at DP6 and propagated inductively very rapidly (simulation, 1.46 m s⁻¹;

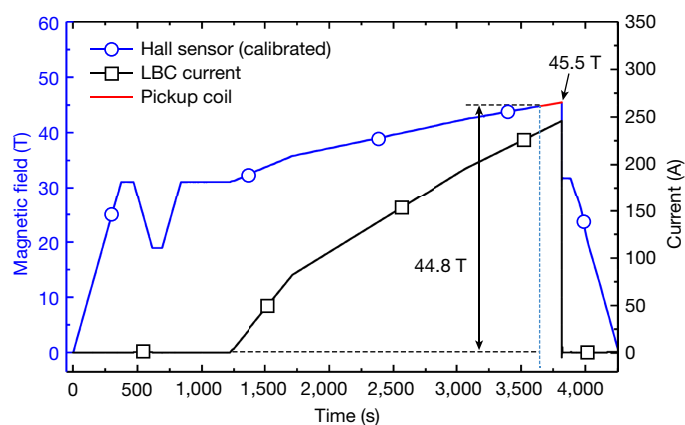


Fig. 2 | Magnetic fields measured at the centre of LBC3 and power-supply current during the test. A calibrated Hall sensor was used up to 44.8 T, and a pickup coil (the linearity of which was confirmed by multiple charging tests before the main test) was used above 44.8 T. LBC3 reached 45.5 T before it quenched at a current of 245.3 A, a conductor current density of 1,420 A mm⁻², a peak magnetic stress of 691 MPa and a total strain of 0.38%.

refinements in the construction of LBC. Like the 45-T magnet, our magnet is also a hybrid, but in this case the superconducting magnet is inside the resistive magnet (unlike the 45-T hybrid magnet, where the 11-T Nb₃Sn superconducting magnet is outside the resistive magnet). Owing to the compact no-insulation design and the ultrathin REBCO tape, the overall winding current density at 45.5 T was 1,260 A mm⁻², nearly five times larger than that of the recently tested HTS/low-temperature superconductor (LTS) 32-T magnet, in which the inner two 17-T solenoids were made from insulated REBCO with a much thicker Hastelloy substrate (50 μm) and higher Cu thickness (100 μm)²⁵.

This test magnet was highly instrumented, allowing many important lessons to be learned for future use. Figure 3 illustrates the voltage behaviour of the six pancake pairs during the 45.5-T quench and shows good agreement between the experimental measurements of the coil voltage and our predictive lumped-circuit model²⁶. The quench was initiated at the DP6 end (DP, double pancake; pancakes P11 and P12) and sequentially propagated by inductive coupling to the top DP (DP6 to DP1) within 0.1 s. Owing to this very fast electromagnetic quench propagation^{27–31}, LBC3—like LBC1 and LBC2—experienced no electrical burn-out. Our simulations predicted a peak temperature of less than 85 K, making damage from heating during the quench very unlikely. However, we noticed increased resistance in several joints after the test and elected to conclude the testing before further quenches so as to perform a ‘post-mortem’ to better evaluate the coil.

In the post-mortem, we unwound each pancake carefully and ran each tape through our continuous-critical-current measuring tool, YateStar³², the principles of which are described in Methods. YateStar

experiment, 1.75 m s⁻¹, almost that of a low-temperature superconductor magnet). Although LBC3 suffered no over-temperature or burn-out during quenching, it did experience mechanical overstrain that we believe is avoidable, as noted in the text.

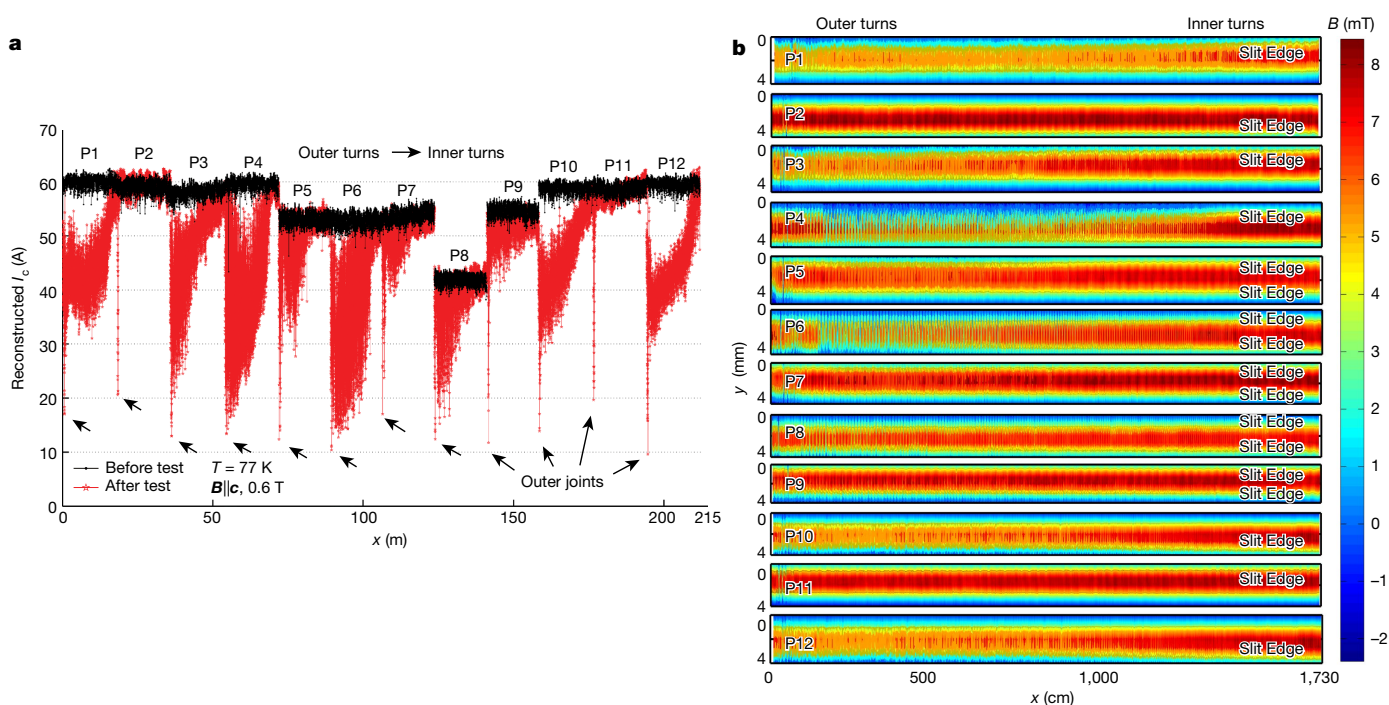


Fig. 4 | Post-mortem analysis of the superconducting tape. **a**, Transport critical current I_c versus position x of the 12 tape lengths before (black) and after (red) the test. $B \parallel c$ indicates that B is perpendicular to the tape plane. **b**, Two-dimensional remnant magnetization maps show the transverse tape uniformity; more uniform (red) tape indicates less damage. 10 of

12 tapes in Fig. 4a show sharply reduced $I_c(x)$ as x increases, whereas the tapes of pancakes P2 and P11 are undamaged. The figure shows that the dominant damage pattern is one-sided, especially for end pancakes P1, P3, P4, P10 and P12. Pancakes P2 and P11, which have slit edges facing the magnet centre, exhibit essentially no longitudinal or transverse damage.

provides a detailed longitudinal and transverse measure of the uniformity of the critical current. We performed YateStar characterizations for LBC3 before winding, after winding and unwinding two pancakes (no damage was seen, and the pancakes were then rewound with the same tape), and finally on all 12 pancakes after the 45.5-T quench. Figure 4a shows that there was evident post-quench degradation of the critical current $I_c(x)$ in most pancakes, but—most importantly—that this damage was absent in pancakes P2 and P11. The majority degradation pattern of $I_c(x)$ increased with increasing radius and

increasing hoop stress, reasonably matching the calculated magnetic strain distribution. Moreover, the outer turns usually had a permanent (that is, plastic) wavy deformation on the conductor edge farthest away from the coil centre. The asymmetric Hall array scans shown in Fig. 4b are associated with preferential penetration of flux into the tape through damaged regions on one side of the conductor, a behaviour that occurred every time that a slit edge faced outwards towards the coil ends. The absence of damage in pancakes P2 and P11 is correlated to the fact that their slit edges faced inwards, towards the coil centre.

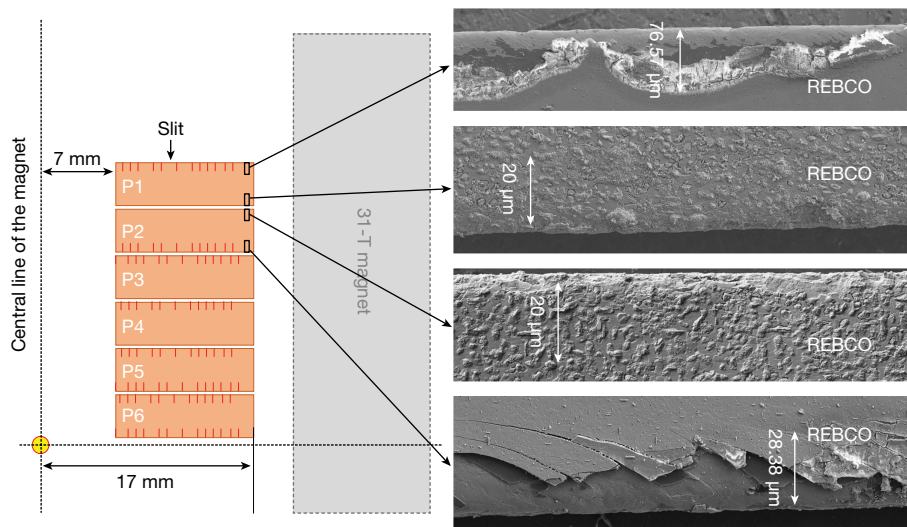


Fig. 5 | Scanning electron microscope images of pancakes P1 and P2 after quenching. The images show the inner and outer (with respect to the magnet centre) conductor edges of P1 and P2. Slit-edge damage is visible in both pancakes, but that on the outer edge of P1 is about three times deeper than that of P2, which has its not-slit edge facing outwards.

The inner edge of P2 is typical of as-delivered tapes. The damage in P1 is the cause of the asymmetric Hall probe scans in Fig. 4b, whereas P2 has an essentially symmetric flux pattern, indicative of uniform current flow uninterrupted by propagated crack damage.

Most interestingly, these pancakes did not exhibit the large hoop-stress damage that reduced I_c to less than half of the inner-turn I_c in most pancakes.

To describe the damage pattern of the tape, we note that the REBCO tapes were made with a width of 12 mm and were then cut into tapes about 4 mm wide, which led to so-called front- and back-slit tapes with one slit edge and middle-slit tapes with two slit edges. Pancakes P5–P9 were wound with such middle-slit tapes, whereas all the other pancakes had back-slit tapes. The key result is that pancakes P2 and P11 had their not-slit edge facing the coil ends, where radial fields were highest and where screening-current stresses and additional out-of-the-tape-plane forces added to the axial hoop tensions, producing unpeeling stresses that could propagate the small cracks generated during slitting³³. These damaged regions are shown in Fig. 5. Therefore, the most important finding of the post-mortem is the survival of pancakes P2 and P11, where cracks did not propagate even in the presence of strong out-of-plane forces. To further test this explanation of the non-uniform damage, we wound three additional single pancakes out of the remaining unused tape and tested two of them in the position of pancake P1, one with the slit edge facing out and one facing in, and with the third one at the magnet centre. As we show in Extended Data Figs. 1, 2, subsequent tests of these coils in the same 31-T magnet fully support the interpretation that orienting the damaged, slit edge towards the interior of the magnet suppresses in-service cracking of the REBCO layer. Accordingly, we believe that the 45-T LBC may be capable of even higher fields when proper attention is given to the positioning and quality of the slit edges. We conclude that, although this test magnet cannot yet be considered as a working user magnet, it does provide a viable route to ultrahigh-field superconducting magnets made from copper oxide high-temperature superconducting conductors.

Online content

Any methods, additional references, Nature Research reporting summaries, source data, statements of data availability and associated accession codes are available at <https://doi.org/10.1038/s41586-019-1293-1>.

Received: 5 June 2018; Accepted: 5 April 2019;

Published online 12 June 2019.

- Miller, J. R. The NHMFL 45-T hybrid magnet system: past, present, and future. *IEEE Trans. Appl. Supercond.* **13**, 1385–1390 (2003).
- Toth, J. & Bole, S. T. Design, construction, and first testing of a 41.5 T all-resistive magnet at the NHMFL in Tallahassee. *IEEE Trans. Appl. Supercond.* **28**, 4300104 (2018).
- Sundaram, A. et al. 2G HTS wires made on 30 μm thick Hastelloy substrate. *Supercond. Sci. Technol.* **29**, 104007 (2016).
- Hahn, S., Park, D. K., Bascuñán, J. & Iwasa, Y. HTS pancake coils without turn-to-turn insulation. *IEEE Trans. Appl. Supercond.* **21**, 1592–1595 (2011).
- Hahn, S. et al. No-insulation multi-width winding technique for high temperature superconducting magnet. *Appl. Phys. Lett.* **103**, 173511 (2013).
- Yoon, S. et al. 26 T 35 mm all-GdBa₂Cu₃O_{7-x} multi-width no-insulation superconducting magnet. *Supercond. Sci. Technol.* **29**, 04LT04 (2016).
- Bascuñán, J., Michael, P., Hahn, S., Lecrevisse, T. & Iwasa, Y. Construction and test results of coil 2 of a three-coil 800-MHz REBCO insert for the 1.3-GHz high-resolution NMR magnet. *IEEE Trans. Appl. Supercond.* **27**, 4300504 (2017).
- Jang, J. Y. et al. Design, construction and 13 K conduction-cooled operation of a 3 T 100 mm stainless steel cladding all-REBCO magnet. *Supercond. Sci. Technol.* **30**, 105012 (2017).
- Liu, J., Wang, L., Qin, L., Wang, Q. & Dai, Y. Recent development of the 25 T all-superconducting magnet at IEE. *IEEE Trans. Appl. Supercond.* **28**, 4301305 (2018).
- Lecrevisse, T. et al. Metal-as-insulation variant of no-insulation HTS winding technique: pancake tests under high background magnetic field and high current at 4.2 K. *Supercond. Sci. Technol.* **31**, 055008 (2018).
- Halperin, B. et al. *High Magnetic Field Science and Its Application in the United States: Current Status and Future Directions* (National Academies Press, 2013).
- Wang, X. et al. Turn-to-turn contact characteristics for an equivalent circuit model of no-insulation REBCO pancake coil. *Supercond. Sci. Technol.* **26**, 035012 (2013).
- Lu, J., Goddard, R., Han, K. & Hahn, S. Contact resistance between two REBCO tapes under load and load cycles. *Supercond. Sci. Technol.* **30**, 045005 (2017).
- Bonura, M. et al. Systematic study of the contact resistance between REBCO tapes: pressure dependence in the case of no-insulation, metal co-winding and metal-insulation. *IEEE Trans. Appl. Supercond.* **29**, 6600305 (2019).
- Kim, S., Hahn, S., Kim, K. & Larbalestier, D. Method for generating linear current-field characteristics and eliminating charging delay in no-insulation superconducting magnets. *Supercond. Sci. Technol.* **30**, 035020 (2017).
- Bai, H., Hannahs, S. T., Markiewicz, W. D. & Weijers, H. W. Helium gas bubble trapped in liquid helium in high magnetic field. *Appl. Phys. Lett.* **104**, 133511 (2014).
- Hahn, S. et al. Field mapping, NMR lineshape, and screening currents induced field analyses for homogeneity improvement in LTS/HTS NMR magnets. *IEEE Trans. Appl. Supercond.* **18**, 856–859 (2008).
- Amemiya, N. & Akachi, K. Magnetic field generated by shielding current in high T_c superconducting coils for NMR magnets. *Supercond. Sci. Technol.* **21**, 095001 (2008).
- Ahn, M. C. et al. Spatial and temporal variations of a screening current induced magnetic field in a double-pancake HTS insert of an LTS/HTS NMR magnet. *IEEE Trans. Appl. Supercond.* **19**, 2269–2272 (2009).
- Koyama, Y. et al. Towards beyond 1 GHz NMR: mechanism of the long-term drift of screening current-induced magnetic field in a Bi-2223 coil. *Physica C* **469**, 694–701 (2009).
- Ueda, H. et al. Measurement and simulation of magnetic field generated by screening currents in HTS coil. *IEEE Trans. Appl. Supercond.* **24**, 4701505 (2014).
- Kajikawa, K. et al. Designs and tests of shaking coils to reduce screening currents induced in HTS insert coils for NMR magnet. *IEEE Trans. Appl. Supercond.* **25**, 4300305 (2015).
- Wang, L. et al. Screening current-induced magnetic field in a noninsulated GdBCO HTS coil for a 24 T all-superconducting magnet. *Appl. Supercond.* **27**, 8200106 (2017).
- Song, J.-B. & Hahn, S. “Leak Current” correction for critical current measurement of no-insulation HTS coil. *Prog. Supercond. Cryog.* **19**, 48–52 (2017).
- Weijers, H. W. et al. Progress in the development and construction of a 32-T superconducting magnet. *IEEE Trans. Appl. Supercond.* **26**, 4300807 (2016).
- Bhattarai, K. R., Kim, K., Kim, S., Lee, S.-G. & Hahn, S. Quench analysis of a multiwidth no-insulation 7-T 78-mm REBCO magnet. *IEEE Trans. Appl. Supercond.* **27**, 4603505 (2017).
- Song, J.-B. et al. Over-current quench test and self-protecting behavior of a 7 T/78 mm multi-width no-insulation REBCO magnet at 4.2 K. *Supercond. Sci. Technol.* **28**, 114001 (2015).
- Yanagisawa, Y. et al. Basic mechanism of self-healing from thermal runaway for uninsulated REBCO pancake coils. *Physica C* **499**, 40–44 (2014).
- Wang, T. et al. Analyses of transient behaviors of no-insulation REBCO pancake coils during sudden discharging and overcurrent. *IEEE Trans. Appl. Supercond.* **25**, 4603409 (2015).
- Markiewicz, W. D., Jaroszynski, J. J., Abramov, D. V., Joyner, R. E. & Khan, A. Quench analysis of pancake wound REBCO coils with low resistance between turns. *Supercond. Sci. Technol.* **29**, 025001 (2016).
- Wang, Y., Chan, W. K. & Schwartz, J. Self-protection mechanisms in no-insulation (RE)Ba₂Cu₃O_x high temperature superconductor pancake coils. *Supercond. Sci. Technol.* **29**, 045007 (2016).
- Coulter, J. Y., Ugurlu, O., Willis, J. O., Holesinger, T. G. & Xie, Y.-Y. Identifying and investigating J_c variations in coated conductors fabricated by MOCVD/IBAD. *APL Conf. Proc.* **1219**, 347–354 (2010).
- Yanagisawa, Y. et al. Remarkable weakness against cleavage stress for YBCO-coated conductors and its effect on the YBCO coil performance. *Physica C* **471**, 480–485 (2011).

Acknowledgements We are grateful to many for help in the coil construction phase, including B. Jarvis (winding), P. Noyes (testing), S. Bole and G. Miller (design), and D. Hazelton at SuperPower Inc. for helping to procure this special coated conductor from early production. This work was performed at the National High Magnetic Field Laboratory, which is supported by National Science Foundation Cooperative Agreement DMR-1644779 and the State of Florida. A part of S.H.'s analysis work was supported by the Samsung Research Funding and Incubation Center of Samsung Electronics under project number SRFC-IT1801-09 and the National Research Foundation of Korea as part of the Mid-Career Research Program (number 2018R1A2B3009249).

Author contributions S.H. and D.C.L. conceived the idea and supervised the work and the writing; S.H. performed the initial electromagnetic and mechanical design of LBC; T.P. and I.D. supervised the coil construction; Kwanglok Kim and Kwangmin Kim contributed to the coil construction and handled the instrumentation; J.J. and T.P. supervised the cryogenic system; K.B., S.N., S.K. and S.H. performed the modelling and analysis; and X.H. performed the coil post-mortem.

Competing interests The authors declare no competing interests.

Additional information

Extended data is available for this paper at <https://doi.org/10.1038/s41586-019-1293-1>.

Reprints and permissions information is available at <http://www.nature.com/reprints>.

Correspondence and requests for materials should be addressed to D.C.L. **Publisher's note:** Springer Nature remains neutral with regard to jurisdictional claims in published maps and institutional affiliations.

© The Author(s), under exclusive licence to Springer Nature Limited 2019

METHODS

Magnet construction. The design of LBC in the resistive magnet (31 T, 50 mm warm bore, 18 MW) is strongly constrained by the 37-mm inner diameter of the helium cryostat. Inner and outer winding diameters of 14 and 34 mm, respectively, and a height of 53.1 mm were chosen. Earlier insulated-winding versions of REBCO coils with Hastelloy and Cu thicknesses of 50 μm and 20 μm , respectively, allowed total fields of 33.8 T (ref. ³⁴) and 35.4 T (ref. ³⁵), the latter at a conductor current density of 508 A mm^{-2} . Making a similar-sized winding that could be safely quenched at much higher current density required a no-insulation winding⁴, the key attribute of which is automatic bypass of the current around hot spots through turn-to-turn contacts; this avoids excessive heating during quenching, which could lead to magnet burn-out^{28–31}. The small 14-mm winding diameter made DP windings (made with a single length of tape, without an inner joint) infeasible, owing to the excessive hard-way bend required at the inner winding bore, and all 12 coils were thus wound as single pancakes with both inner and outer resistive joints to electrically connect adjacent pancakes. The tape was wound with the REBCO layer facing radially inwards to provide compressive bending strain to minimize the overall strain produced by the tensile Lorentz forces. An inner Cu winding support tube acted as current lead for the bottom pancake (Fig. 1), making LBC very compact. A separate copper current lead was connected to the top pancake.

After winding, the 12 pancakes were axially compressed with a preload of 86 kg provided by three parallel sets of Belleville washers, as shown in the schematic in Fig. 1. To mitigate hot spots (due to diamagnetic levitation of helium liquid, leading to trapped helium gas bubbles around the end windings¹⁶) during the test, great care was taken with the joints so as to generate the minimum heat possible. Inner joints had resistance values (measured in liquid nitrogen before the main test) of 0.05–0.98 $\mu\Omega$, and outer joints had 0.04–2.1 $\mu\Omega$.

Magnet testing. We found that liquid nitrogen tests were valuable for checking joint resistances and establishing key operation parameters, including the coil constant, the characteristic coil resistance R_c and the charging time constant^{12–15}. Occasionally some joints were remade to reduce resistive losses and minimize coil warming during the test. For the high-field test, LBC3 was placed in a 37-mm-diameter liquid-helium cryostat inside the resistive background magnet (50-mm warm bore, 18 MW, 31.1 T) at MagLab. To mitigate the trapped helium bubbles¹⁶, a small-diameter tube was placed above the magnet, and the helium vapour was pumped away during the test so as to limit the temperature of the top surface of LBC3 to 7 K at the moment of the 45.5-T quench. A Hall sensor that was calibrated up to 44.8 T in the existing 45-T hybrid magnet was used to measure the centre field of LBC3, together with a pickup coil; the linearity of the pickup coil was confirmed by comparing the fields measured by the pickup coil with those measured by the calibrated Hall sensor in multiple charging tests before the main 45.5-T test.

Hall probe array measurements of the uniformity of the tapes. The data in Fig. 4 were all taken in our combined transport and magnetization tape evaluation instrument, YateStar, which allows continuous scanning of the critical current I_c at 77 K with a resolution of about 2 cm while passing the tape through two magnets applying fields of 0.6 T perpendicular and parallel to the tape, thus allowing measurement of the I_c anisotropy. The transport-current measurement gives an integrated measure of the longitudinal distribution of I_c , but cannot define the transverse distribution. The transverse distribution can be deduced from the remanent-field screening-current distribution, which was measured by an array of seven Hall probes, spaced about 0.5 mm apart and placed above the tape between the two magnets. These measured the local field due to the screening currents, which would be symmetrical and peak in the centre for a uniform critical current density distribution^{36,37}. This colour visualization gives an immediate indication of whether localized damage is present or not. Pancakes P2 and P11 in Fig. 4b show an essentially uniform and symmetrical colouring along their whole lengths, whereas the highest field (red, about 8 mT) corresponds to the trapped field of the remanent screening currents in the tape centre, which proves the lack of any substantial

damage in these tapes, which is also consistent with the transport measurements in Fig. 4a. By contrast, other tapes (for example, those in pancakes P1 and P12) show transport I_c distributions that degraded considerably from the inner to the outer winding turns of the coil, largely due to the $\sigma_\theta = BJR$ magnetic stresses that increase from the inner to the outer turns. This damage becomes progressively more asymmetric owing to preferential damage on the outer slit edges. The induced screening-current stresses also play a major role in the asymmetric damage pattern and the consequent plastic rippling of most of the tapes. This damage is shown in Fig. 5.

Subsequent single-pancake tests. To test our hypothesis that conductor damage at the high stresses of our 45.5-T coil occur only when the slit edge points towards the exterior of the coil, we made three subsequent test coil sets, named Coil A, B and C. In the first of these sets, we made single-pancake test coils out of the same 30- μm -substrate tape used in the three LBC series magnets, but in this case all lengths had only one slit edge. The geometry of these three coils is shown in Extended Data Fig. 1. Two of the coils (A and B) were placed in a position similar to that of pancake P1 in LBC3 in the 31-T magnet, whereas coil C was placed in the central field region corresponding to pancakes P6 and P7. Each length of tape was run through YateStar before winding and after the tests. Coils A and B were built to investigate the effect of the radial field and were placed 100 mm above the centre of the 31-T magnet, where the radial field was the largest (about 1.6 T). In the tests of all of the three coils, the current ramp rate was 1 A s^{-1} for a target current below 200 A and 0.5 A s^{-1} for higher target currents. During unwinding of the coils, the tapes were unsoldered from the current leads, and some damage occurred during unsoldering.

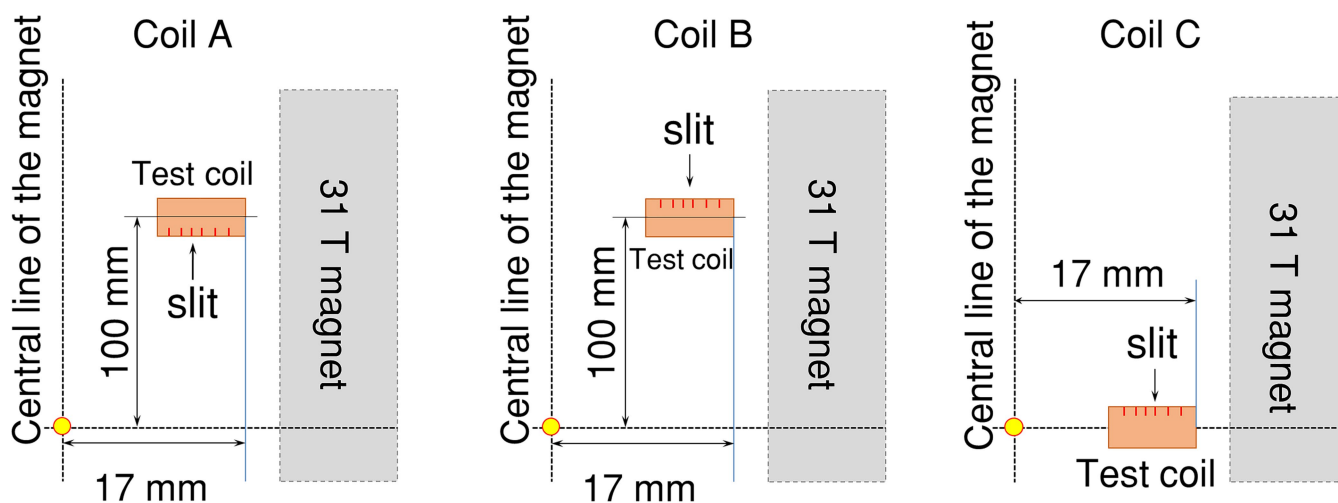
Extended Data Fig. 2 shows two-dimensional Hall magnetization maps before (upper) and after (lower) the high-field tests and their reconstructed transport critical current I_c (77 K, $B \parallel c$, 0.6 T) for coils A, B and C. None of the coils was quenched. Coils A and B were cycled eight and five times, respectively, between 225–250 A in a background field of 31 T. The peak hoop strain (magnetic plus bending) was 0.27%. Coil A showed no I_c degradation, but coil B developed obvious damage on its slit edge (see circled region), and this edge also suffered permanent rippling damage. The arrowed defects in coil B have a period matching the coil circumference, which we attribute to a periodic stress concentration. Coil C was cycled five times between 220–240 A and 240–250 A. The current was raised to 295 A at the end of the test, which corresponds to a combined magnetic and bending hoop strain of 0.5%.

Collectively these three tests show that damage was only seen for the coil in the high-radial-field position and only when the slit edge was facing outwards in the damaging orientation. Damage was absent when the slit edge was facing inwards and not seen in the centrally placed pancake even when the maximum magnetic-plus-bending strain was 0.5%, that is, even greater than that of LBC3 (0.38%). The results demonstrate that the proper edge orientation of pancakes wound with REBCO conductor has an important role in suppressing mechanical damage in high-field REBCO magnets.

Data availability

The data that support the findings of this study are available from the corresponding author upon reasonable request.

- Markiewicz, W. D. et al. 33.8 tesla with a $\text{YBa}_2\text{Cu}_3\text{O}_{7-x}$ superconducting test coil. *AIP Conf. Proc.* **1218**, 225–230 (2010).
- Trociowitz, U. P. et al. 35.4 T field generated using a layer-wound superconducting coil made of (RE) $\text{Ba}_2\text{Cu}_3\text{O}_{7-x}$ (RE = rare earth) coated conductor. *Appl. Phys. Lett.* **99**, 202506 (2011).
- Brandt, E. H. & Indenbom, M. Type-II-superconductor strip with current in a perpendicular magnetic field. *Phys. Rev. B* **48**, 12893–12906 (1993).
- Furtner, S., Nemetschek, R., Semerad, R., Sigl, G. & Prusseit, W. Reel-to-reel critical current measurement of coated conductors. *Supercond. Sci. Technol.* **17**, S281–S284 (2004).



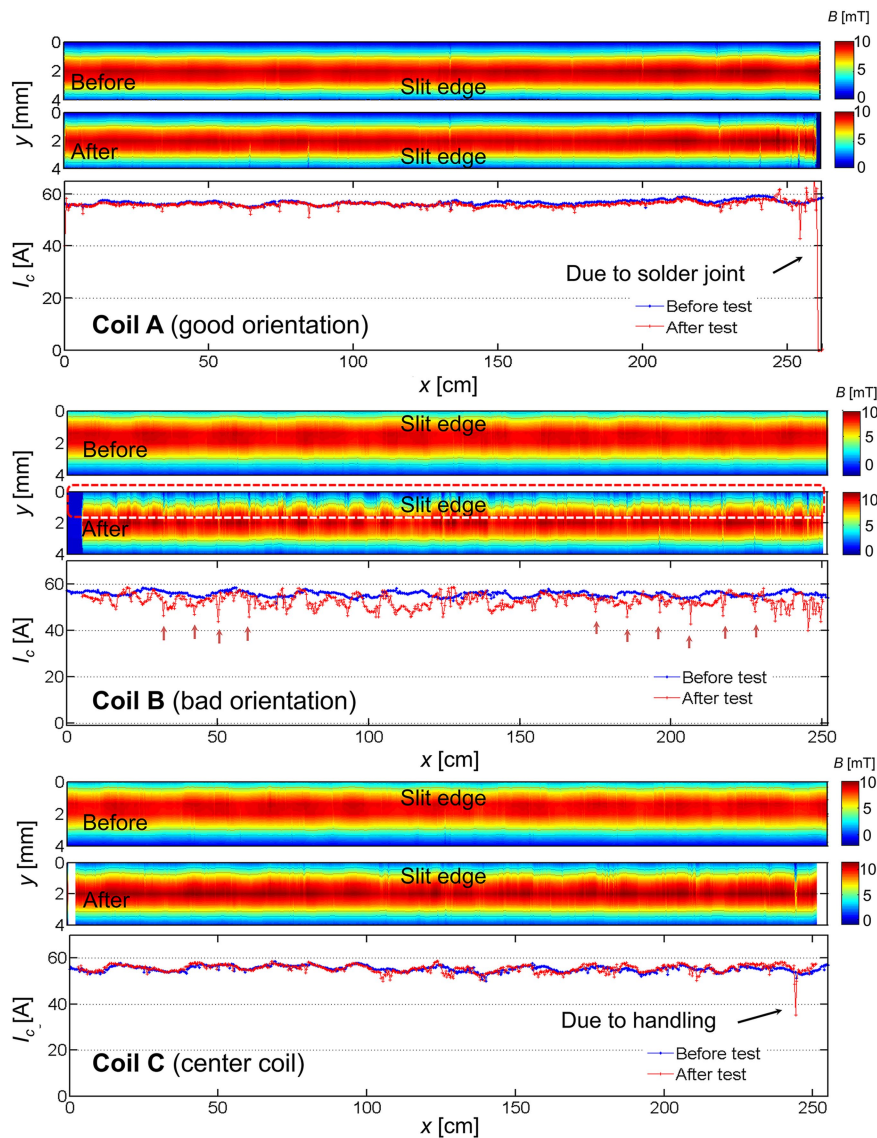
* Not to scale

Extended Data Fig. 1 | Geometry of three single pancake test coils.

The test coils were made with the same 30- μm -thick substrate tape used in LBC3 and were built to simulate the outermost 25 turns of LBC3. The tapes in Coil A and Coil B have only one slit edge, where their orientation and position is varied from the supposed damage-free orientations of Fig. 4. Coil A is positioned with its slit edge facing inwards towards the

magnet centre, whereas Coil B has the reverse and unsafe orientation.

Coils A and B are placed into the same 31-T magnet used for the LBC3 coil test in a position similar to that of pancake P1, where the radial field is highest. Coil C is placed in the central field region, where the radial field is essentially zero and only hoop tension operates, mimicking the central pancakes P6 and P7.



Extended Data Fig. 2 | Two-dimensional Hall magnetization maps and reconstructed transport critical current, I_c . The maps were obtained for coils A, B and C before (top) and after (bottom) the high-field tests, and I_c was reconstructed for 77 K, $B||c$ and 0.6 T. None of the coils was quenched. Coils A and B were cycled eight and five times, respectively, between 225–250 A in a background field of 31 T. The peak hoop strain (magnetic plus bending) was 0.27%. Coil A showed no I_c degradation, but coil B

developed obvious damage on its slit edge (see circled region), which also suffered permanent rippling damage. The arrowed defects in coil B have a period matching the coil circumference, which we attribute to a periodic stress concentration. Coil C was cycled five times between 220–240 A and 240–250 A. The current was raised to 295 A at the end of the test, which corresponds to a hoop strain of 0.5%.